

Fast Magnetic Coil Controller for Cold Atom Experiments

L. Uhthoff-Rodríguez, E. G. Alonso-Torres, A. Hernández-López, E. Esquivel-Ramírez, G. Carmona-Torres, C. Gardea-Flores, J. A. Seman, and A. Paris-Mandoki^{a)}
Instituto de Física, Universidad Nacional Autónoma de México, Ciudad de México C.P. 04510, Mexico

(Dated: 31 March 2025)

Cold atoms experiments employ magnetic fields, commonly generated by coils, as an essential tool to control and manipulate atomic samples. In these experiments, it is often necessary to rapidly switch the magnetic field between two values. However, typical power supplies have a limited switching time for the current flowing through the coil that is inversely proportional to the maximum voltage they can supply and directly proportional to the inductance of the coil. We present a control scheme implemented as an electronic circuit that overcomes this limitation, a faster control is achieved by momentarily applying an on-demand high voltage when the control signal variation surpasses the limits that the conventional power supply can follow, allowing a faster current flow into the magnetic coil. In our specific application, we show that with this control the coil current can follow control signals continuously from negative to positive and vice versa with a ~ 5 kHz bandwidth and a maximum switching speed of ~ 40 μ s between -1 A and 1 A even though the time constant of the coil is of ~ 2 ms. Improving by more than a factor of ten the bandwidth and making the switching speed 20 times faster than that of a typical power supply. By appropriately selecting the components of the circuit, the switching time and the bandwidth can be finely tuned to any desired value. Moreover, our scheme can be easily adapted to different applications within a wide range of inductive and power requirements.

I. INTRODUCTION

Cold atom experiments stand out for the breathtaking level of control they allow. Indeed, these setups have made it possible to manipulate individual atoms¹⁻³, ions⁴⁻⁶, and photons⁷.

To achieve this sophisticated degree of control, one of the most important tools is magnetic fields, since they play a central role in many of the techniques employed for creating and manipulating the cold atomic samples. Such is the case of laser cooling techniques⁸, the creation of magnetostatic⁹ and magneto-optical¹⁰ traps; magnetic transport of atoms across an experimental setup¹¹; optical pumping and fine control of hyperfine states¹²; control of interatomic interactions in the ultracold regime by means of a magnetic Fano-Feshbach resonance¹³, and even the cancellation of external undesired fields¹⁴ to implement sub-Doppler cooling¹⁵⁻¹⁷ or for high-resolution spectroscopy techniques such as those used in atomic clocks¹⁸⁻²⁰.

Magnetic coils are by far the most widely used method in these experiments to generate magnetic fields, as they offer the possibility of manipulating the intensity and direction of the field, and even extinguishing it completely. For this reason, it is crucial to develop electric and electronic circuits that allow to control the current that passes through the coils in a very precise and versatile fashion.

In particular, many of the processes employed in cold atoms experiments require to abruptly switch the field between two different values. For instance, laser cooling often involves a stage in which atoms are trapped

in a magnetic field and then further cooled down after abruptly switching the field off with processes known as optical molasses^{8,21,22}. Experiments with atomic Fano-Feshbach resonances sometimes require a very fast sweep (below 100 μ s) between two values of the magnetic field^{23,24}. Another example is the spin-echo technique, used to characterize cold atoms, a sequence of few millisecond pulses of magnetic field is employed²⁵.

However, a common limitation of magnetic coils concerns, precisely, the switching time between two states of the magnetic field. Both, the inductance of the system and the limited maximum voltage of the current supply of the coils, considerably increases the time in which the field can be varied, making it difficult to switch it abruptly. In this paper we present an electronic circuit that effectively overcomes this difficulty. The components of the presented circuit have been chosen for the application of quickly changing the current in shim coils used to compensate external magnetic fields or to set a small bias field to define a magnetization axis for optical pumping¹². Nonetheless, the circuit can be adapted to other applications by sizing the components accordingly.

The coils used for producing magnetic fields in cold-atom experiments typically have resistances of, at most, a few ohms and the power supplies used for driving them are optimized for large steady-state current while the voltage limit is of a few volts. For a given power supply with a voltage limit of V_{\max} , the maximum increase in current that can be achieved for a coil of inductance L is $\frac{dI}{dt} = V_{\max}/L$. In this work, we present a circuit that regulates the current passing through magnetic coils and allows overcoming this limit enabling faster control over them. To achieve this, a high voltage and low current supply is used to charge capacitors, which can then provide a high current at high voltage for short periods of time and complement the steady-state power supply

^{a)}Electronic mail: asaf@fisica.unam.mx

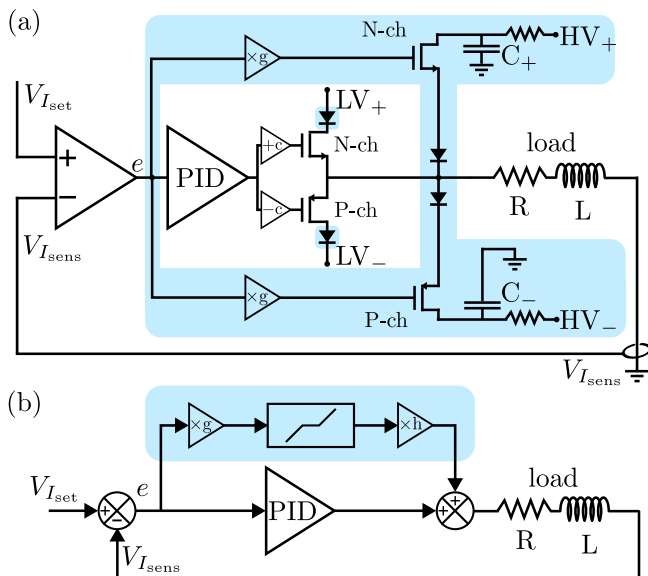


FIG. 1. **Simplified diagrams of current regulator.** The unshaded region shows the basic current regulating circuit and the shaded region includes the additions that enable fast switching. (a) Circuit schematic, (b) block diagram. The triangular symbols with $\times g$ or $\times h$ apply a gain with factor g or h respectively and the triangular symbols with $\pm c$ apply an offset of c to the signal to cancel the gate threshold voltage $V_{GS(th)}$ of each MOSFET.

during changes of the current set point, shortening the time of the transient behavior. A drawback of this circuit is that it requires a charging period to prepare for fast dynamic changes in the set current. However, this limitation is compatible with most cold-atom experiments, which also require a charging period to collect cooled atoms, where the currents are kept constant before executing an experimentation and measurement sequence.

II. PRINCIPLE OF OPERATION

A simplified schematic of the circuit is presented in Fig. 1a. This circuit is powered by two separate power supplies: a “low voltage” (LV) that can output a large current, which drives the load during steady state, and a “high-voltage” (HV) supply that is used to charge the capacitors C_+ and C_- that drive the fast switching part of the circuit. We will begin by describing the basic current regulating circuit (unshaded) and then detail the fast switching section (shaded). The actual value of the current passing through the load is measured with a current sensor that outputs a voltage $V_{I_{sens}}$ which is compared to the desired set voltage $V_{I_{set}}$. The resulting error signal $e = V_{I_{set}} - V_{I_{sens}}$ is fed into a PID (proportional-integral-derivative) controller that drives a pair of complementary N- and P-channel MOSFETs arranged in a push-pull configuration. In this configuration, when $V_{I_{set}} > V_{I_{sens}}$ the output voltage of the PID controller increases causing

the conductivity of the N-channel MOSFET to also increase so that more current flows from LV_+ to the load until $V_{I_{set}} \approx V_{I_{sens}}$. Conversely, for $V_{I_{set}} < V_{I_{sens}}$ the PID controller also adjusts its output until $V_{I_{set}} \approx V_{I_{sens}}$ by increasing, now, the conductivity of the P-channel MOSFET. Before being fed to the gates of the LV MOSFETs, the output of the PID is offset by the conduction threshold voltage of each MOSFET ($V_{GS(th)}$) so that there is no dead-zone, meaning that they begin conduction as soon as the PID output starts deviating from zero. This offset can even exceed by a small margin the threshold voltage resulting in some power dissipated at the LV MOSFETs but at the same time providing some immunity from fluctuations in the threshold voltages. Because the MOSFETs are complementary, only one of them conducts current at any given time. As the relationship between the gate voltage and the conductivity of the MOSFETs is not always linear, and it may even be different for the N- and the P-channel MOSFETs, we employ the PID controller to ensure that the linearity of the circuit is only limited by the linearity of the current sensor.

The fast switching part of the circuit shown in the shaded part of Fig. 1a contains two capacitors that are charged to high voltage which can be negative (HV_-) or positive (HV_+). The discharge of these capacitors towards the magnetic coil load is controlled by an additional pair of MOSFETs, also arranged in a push-pull configuration. The diodes shown in schematic are there so that the current from the HV supply does not flow into the LV supply and vice versa. As opposed to the LV part of the circuit, the power MOSFETs for the HV part are driven directly by the error signal and there is no offset added to it so they only become active when the magnitude of the error signal is larger than the MOSFETs’ conduction threshold voltage $V_{GS(th)}$. As a result, the HV part of the circuit is inactive when the circuit is in a steady state and the error signal is close to zero. For an abrupt change in the current set point $V_{I_{set}}$, the error signal changes accordingly and allows current to flow from an HV capacitor to the load. As the voltage of the capacitors is much larger than the LV one, a higher $\frac{dI}{dt}$ can be attained and therefore a faster switching time. Once the switching has completed and the error signal approaches zero the HV part of the circuit becomes inactive again and the LV power supplies take over. While the load is being supplied by the capacitors their voltage decreases and they become less effective. For this reason this type of design is only useful if the application is compatible with a down time that allows the capacitors to charge.

The behavior of the circuit in a typical application is shown in Fig. 2. Here, a short (2 ms) pulse sequence is executed once per second and the delay between pulses allows the capacitors to charge. For the measurements shown in this paper, we used a coil with $L = 550 \mu\text{H}$ and $R = 0.26 \Omega$ resulting in a natural time constant $\tau = L/R = 2.1 \text{ ms}$. As can be seen in Fig. 2a, the capacitor voltages C_+ and C_- asymptotically approach $\pm 30 \text{ V}$ during the charging period and drop when the

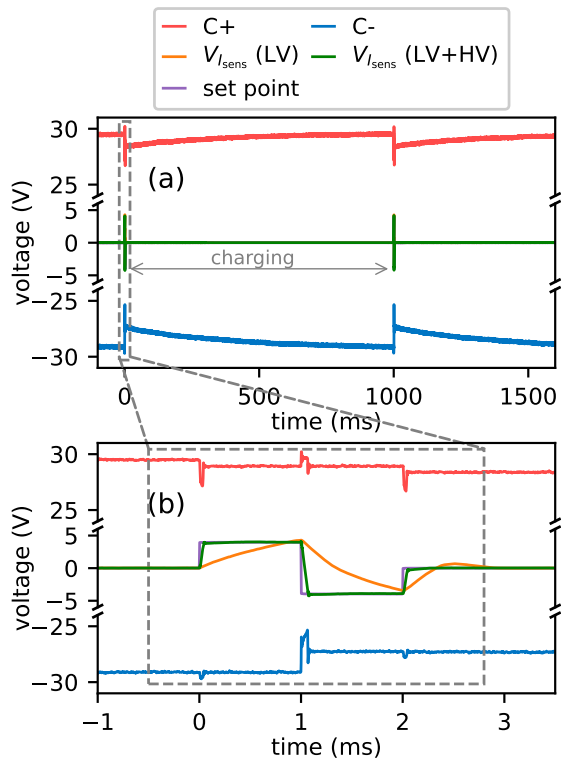


FIG. 2. **Typical operation of the circuit.** The behavior in time of the voltage in the positive (C_+) and negative (C_-) capacitors, and current in the inductive load when the current set point is changed. The current is plotted for two different cases: when only the low-voltage supply is used (LV) and when the low and high-voltage supply are used in combination (LV + HV). (a) Long-term behavior of the circuit. A short pulse sequence is executed at time = 0 which depletes the capacitors and is followed by a 1 s wait to allow the capacitors to charge before executing the pulse sequence again. (b) Detailed view of the execution of the time sequence over a short interval around switching events. The charging voltage of the capacitors is ± 30 V and the scale of the current sensor that measures $V_{I_{\text{sens}}}$ is 4.3 V/A.

pulse sequence is executed at 0 ms and at 1000 ms. A more detailed view of the pulse sequence during a short interval around $t = 0$ can be observed in Fig. 2b. Here, a comparison is made between the circuit operating only with the LV part active and when both the LV and HV parts are used. When using only the LV part the value of the current can not even settle before the set point has already changed while the case with both LV and HV responds much faster and can follow the set point better. In the detailed view of the capacitor traces C_+ and C_- in Fig. 2b it can be seen that when the set point jumps upwards the charge of the positive capacitor is used to drive the current and it is, therefore, left with a lower charge after the jump. For downward jumps the negative capacitor is depleted. Additional to the changes in the C_+ and C_- voltages due to the decrease in their charge, there are some transient ($\lesssim 0.1$ ms) jumps that occur during

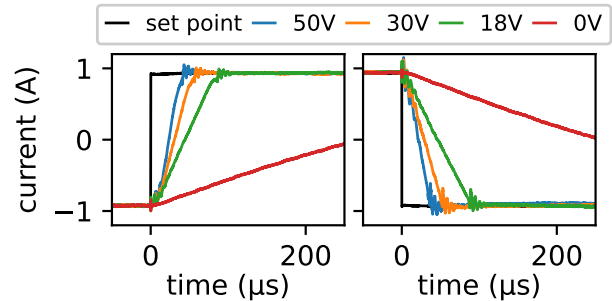


FIG. 3. **Step response of the current.** Response of the current for a rising (left) and falling (right) edge on the set point for different voltages in the HV supply. The 0 V indicates the case where only the LV part of the circuit is used.

the activation of the HV part of the circuit which do not meaningfully affect the capacitor charge since the value before and after the transients is the same when the capacitors charge is not used to supply the current.

III. TIME-DOMAIN RESPONSE

To further investigate the switching behavior of the circuit we measure the step behavior for a rising edge and a falling edge for different voltages used for the HV supply. The current was switched from -1 A to 1 A and the obtained results are presented in Fig. 3. The test with the HV part disabled is indicated as 0 V, in this case it takes $900 \mu\text{s}$ for the current to reach the set point and further $400 \mu\text{s}$ for it to settle (extending beyond the figure). With the HV circuit enabled, the switching occurs at a much shorter time scale and increasing the capacitor charge voltage, further reduces the switching time.

While using higher voltages for switching the current can greatly improve the switching time, this cannot be used for arbitrarily complex pulse sequences due to the finite amount of charge stored in the capacitors. This limitation is demonstrated in Fig. 4, where a long sequence of square pulses is presented. Whenever the set point is increased or decreased, the positive or the negative capacitor is discharged respectively and therefore their voltage also decreases in absolute value. With decreased voltage the speed-up in switching time also decreases until there is no improvement at all and by the end the output follows a sawtooth behavior instead of a square wave. Moreover, even though the pulse sequence used in this measurement was symmetrical with respect to 0 V the remaining charge in the capacitors at the end of the sequence is different. This may be caused by specific differences between the N- and P-channel MOSFETs used in the HV part, such as differences in resistance when switched completely on (R_{ON}) or in their gate capacitance.

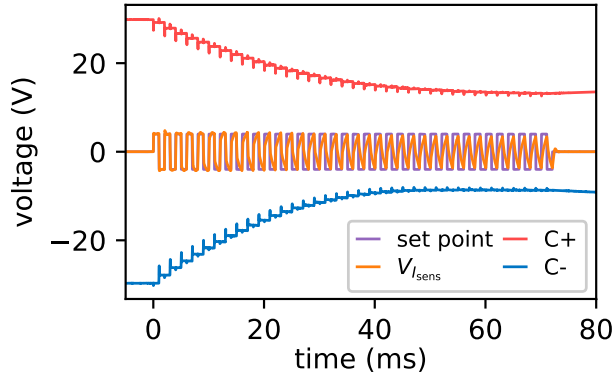


FIG. 4. **Limitations of the fast switching circuit.** A sequence of many square pulses is used as set point for the circuit. A stepwise discharge of the capacitors is observed. As the capacitor voltage decreases, the effectiveness of the circuit is reduced. The scale of the current sensor that measures $V_{I_{\text{sens}}}$ is 4.3 V/A.

IV. FREQUENCY-DOMAIN RESPONSE

To gain further understanding of this circuit we also studied it in the frequency domain. A sinusoidal signal was used as the input for the set point of the current $V_{I_{\text{set}}}$ and the resulting oscillating current in the load was measured using the current sensor in the circuit to obtain $V_{I_{\text{sens}}}$. Then, for each frequency f of the input, both the input and output signals were fit to $A \sin(2\pi ft - \phi) + B$ to get the gain $|A_{\text{out}}/A_{\text{in}}|$ and phase-shift $\Delta\phi = \phi_{\text{in}} - \phi_{\text{out}}$ to obtain the response function²⁶. For this measurement the system was allowed to reach a steady-state at a constant set point before sending the oscillating stimulus so that the HV capacitors started the sequence fully charged. During the analysis we only used the first two sinusoidal periods of the signals to avoid the capacitors' depletion affecting the measurements. The results are presented in Fig. 5. To quantify the bandwidth limitation of the control electronics we first measured the response of the circuit for the case where the load was purely resistive and of low resistance avoiding the delays caused by an inductive load. The results of this case are labeled as “short” and bandwidth of ~ 100 kHz was obtained. Once the inductive load was introduced, we first measured with only the LV part of the circuit active (shown as “coil 0 V”) obtaining a bandwidth of ~ 500 Hz. With the HV part of the circuit enabled we observe an increase in bandwidth by more than a factor of 10 when considering both the point of 3 dB decrease in gain or when the phase shift begins to decrease rapidly with frequency around ~ 10 kHz. Again, with higher HV voltage there is a larger increase in bandwidth. This is consistent with step measurements of Fig. 3 since the more frequency components available to reproduce a step function, the

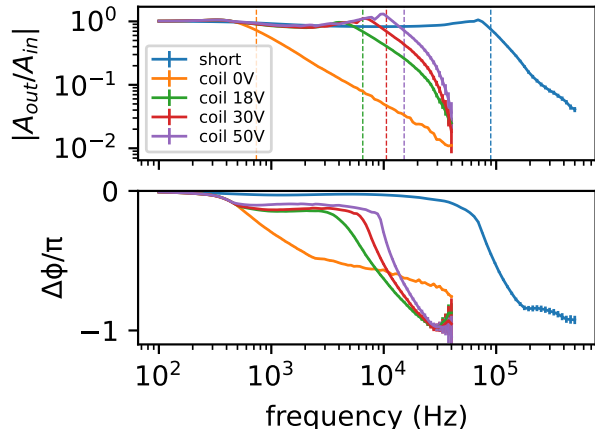


FIG. 5. **Short-term response function.** A sinusoidal input was used as the set point of the circuit and the output gain and phase-shift of the first two periods was measured. The “short” plot indicates the case where a short wire was used as the load instead of a coil with significant inductance. The “coil 0 V” shows the case with the coil and only the LV part of the circuit active (the HV part is disabled). The following measurements “coil 18 V”, “coil 30 V” and “coil 50 V” show when both the LV and HV parts of the circuit are active and the indicated voltage is the one used to charge the capacitors. Vertical dashed lines indicate the bandwidth cutoff frequencies, where the signal magnitude decreases by 3 dB.

shorter the rising and falling times will be. At low frequency, the response of all the cases with inductive load is identical since the HV part of the circuit does not activate. To activate the HV part it is required that the error signal overcomes a threshold and for slow signals, the LV part is fast enough to follow the set point. Only when the LV part of the circuit begins to falter the HV activates.

To understand why the bandwidth increases when activating the HV section, the dynamical system²⁷ represented by the block diagram shown in Fig. 1b is a good approach for analysis. The shaded region shows that the error signal gets amplified by a factor g , then there is a dead-zone block that models the voltage threshold $V_{\text{GS(th)}}$ required by each HV MOSFET to start conducting. Finally another gain stage by a factor h models both the HV MOSFETs and the charged capacitors. The amplified signal is then added to the output of the PID to drive the load. It is important to note that this model is only valid for short pulse bursts, since for longer times the capacitors discharge effectively decreasing the h gain as in Fig. 4. The overall effect of the shaded part of the circuit is that, whenever the error signal overcomes the threshold set by the dead-zone, the proportional gain of the feedback circuit is increased to $\approx K_p + gh$, where K_p is the proportional gain of the PID in the LV part of the circuit. When the gain inside a control loop is increased, the system can follow the set point more closely and the

bandwidth is effectively increased²⁶.

V. SCALING AND LIMITS

A feature of this circuit is that shorter switching times can be achieved by increasing the capacitor charging voltage which could even be in the range of several kV when using a switched-mode power supply such as a DC-DC converter. However, there are several practical limitations to using such high voltages which will ultimately constrain scaling this solution: i) For MOSFETs, their resistance when switched completely on, R_{ON} , grows as the square of the maximum rated voltage that the MOSFET can handle²⁸. Therefore, when increasing the voltage rating, at some point the dissipated power might become unmanageable. ii) Capacitor with both a high breakdown voltage and a high capacitance are uncommon so a large array of capacitors may be required. iii) Higher voltage circuits also require special design considerations in the geometry and spacing of the PCB traces as well as conformal coating to prevent insulation breakdown²⁹.

The selection of the required capacitors is very application dependent. For a use case where only a small jump in current is required every few seconds a small capacitor may suffice while for a complex sequence a larger capacitance may be required. This would slow down the voltage decrease on the capacitors but will also take a longer time to charge them for the same output current of the HV supply.

When designing an electromagnet to achieve a specific magnetic field B_0 in a given geometry, the product I_0N of the required current delivered to the coil I_0 and the number of windings N is fixed by B_0 . A coil with many windings and a small current would produce the same field as one with few winding and a large current. For experiments where a fast switching of the coils is desirable, the number of windings is minimized at the expense of increased current requirements, and increased wire thickness, to decrease the inductance of the coil. In the context of this circuit the choice of fewer windings has the additional advantage that the voltage drop at the coil in the steady-state operation (the LV part) is small. If, instead, the coil required large voltages even for the steady-state operation, then the HV part of the circuit would not provide such a great advantage. Additionally, the maximum voltage that can be applied to the coil is bounded in the presented implementation by the voltage range of the PID control electronics to drive the LV MOSFETs. Since many magnetic coils designed for cold atom experiments are already optimized for fast on-off switching by minimizing inductance, they are well-suited for applications using this circuit.

VI. CONCLUSIONS

The presented design consists of two pairs of MOSFETs, each in a push-pull configuration and working together in a coordinated manner. One regulates the current from the LV supply and has the typical performance of circuits driving magnetic coils in cold atom experiments. The second pair, which provides current from capacitors charged to a HV, results in a high improvement to the controller in terms of switching time and bandwidth. Switching time is reduced as shown in Figs. 2 and 3 while bandwidth is improved by a factor of ten with respect to the ~ 500 Hz bandwidth when only the LV circuit is enabled.

This circuit is a solution to control abrupt current steps including changes in current direction. Moreover, it can follow arbitrary control signals that are within the demonstrated bandwidth and the limitation of cycles needed to discharge the capacitors. It can be adapted to magnetic coils in cold atoms experiments that are normally driven by power supplies which are limited to deliver a large steady-state current operating at low voltages. By an appropriate component selection it can be adapted for different needs by changing the capacitors, MOSFETs and tuning the HV activation threshold. More consecutive current pulses can be achieved with larger capacitors while a faster reset of the circuit's operating state is obtained when using capacitors with lower capacitance. In other words, the great versatility of our proposal allows it to be adapted to a wide variety of situations, depending on the user's needs.

The demonstrated fast control opens the possibility of implementing improved experimental sequences by allowing more agile progress through the different experimental stages. It can also improve existing cooling and state-preparation stages and allow the exploration of different physical regimes in which the time required for magnetic fields to change must be as short as possible. For example, experiments in which the inter-particle interaction is controlled by a magnetic field via a Fano-Feshbach resonance, can greatly benefit from our scheme, as it allows avoiding delay times and the resulting decrease in the cloud's phase-space density, since the waiting time to reach the desired magnetic field can be significantly reduced.

Appendix: Full Schematic

The full schematic is shown in Fig. 6 and the work files can be obtained from³⁰. In this circuit several parameters can be adjusted such as the different gains of the PID controller, the attenuation of both feedback and the set point, the activation threshold of the HV section and the offset added to the PID output to avoid a dead-zone in the LV section.

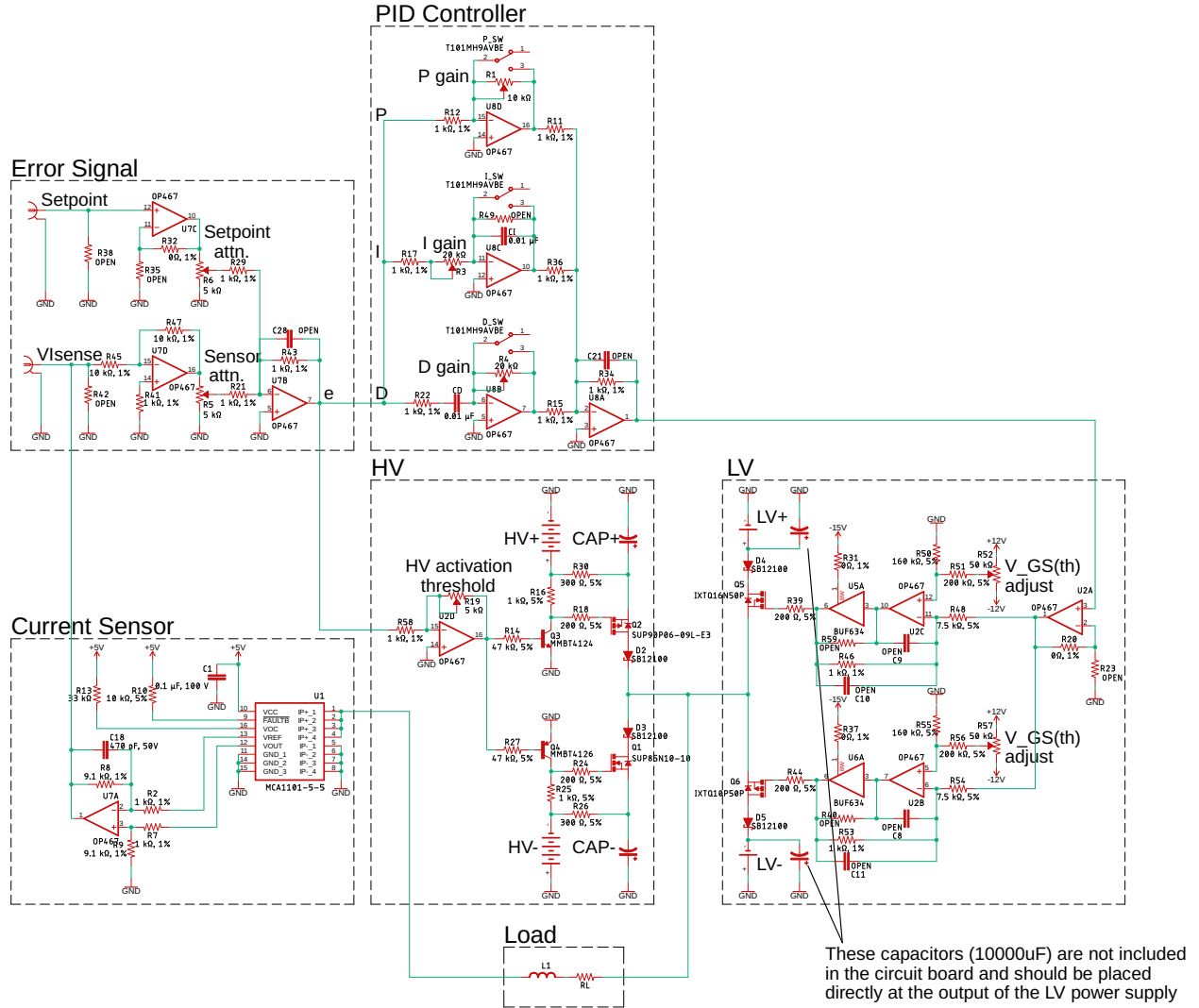


FIG. 6. Full schematic of the circuit. The work files and PCB layout can be obtained from the repository³⁰.

ACKNOWLEDGEMENTS

The authors would like to acknowledge Alan Stummer for publishing the circuits he developed for magnetic coil switching which served as an inspiration, Michael Schlagmüller whose original PID circuit design we adapted in this circuit and Rodrigo Alejandro Gutiérrez Arenas for early discussions on conceptualizing this work. This work was supported by the UNAM-CIC LANMAC program. J. A. S. acknowledges support from UNAM-PAPIIT

IN105724 and SECIHTI CF-2023-I-72 and A. P.-M. acknowledges support from UNAM-PAPIIT IN115523. L. U.-R., E. G. A.-T., A. H.-L., E. E.-R., and G. C.-T., acknowledge fellowships from SECIHTI for their graduate studies.

¹N. Schlosser, G. Reymond, I. Protsenko, and P. Grangier, *Nature* **411**, 1024 (2001).

²A. M. Kaufman and K.-K. Ni, *Nat. Phys.* **17**, 1324 (2021).

³J. F. Sherson, C. Weitenboer, M. Endres, M. Cheneau, I. Bloch, and S. Kuhr, *Nature* **467**, 68–72 (2010).

- ⁴W. Neuhauser, M. Hohenstatt, P. E. Toschek, and H. Dehmelt, *Phys. Rev. A* **22**, 1137 (1980).
- ⁵D. Wineland and W. M. Itano, *Phys. Lett. A* **82**, 75–78 (1981).
- ⁶C. Zipkes, S. Palzer, C. Sias, and M. Köhl, *Nature* **464**, 388–391 (2010).
- ⁷D. E. Chang, V. Vuletić, and M. D. Lukin, *Nat. Photonics* **8**, 685 (2014).
- ⁸H. J. Metcalf and P. V. der Straten, *Laser Cooling and Trapping* (Springer, New York, 1999).
- ⁹T. Bergeman, G. Erez, and H. J. Metcalf, *Phys. Rev. A* **35**, 1535 (1987).
- ¹⁰A. L. Migdall, J. V. Prodan, W. D. Phillips, T. H. Bergeman, and H. J. Metcalf, *Phys. Rev. Lett.* **54**, 2596 (1985).
- ¹¹M. Greiner, I. Bloch, T. W. Hänsch, and T. Esslinger, *Phys. Rev. A* **63**, 031401 (2001).
- ¹²W. Happer, *Rev. Mod. Phys.* **44**, 169–249 (1972).
- ¹³C. Chin, R. Grimm, P. Julienne, and E. Tiesinga, *Rev. Mod. Phys.* **82**, 1225 (2010).
- ¹⁴D. O. Sabulsky, *Rev. Sci. Instrum.* **95**, 081401 (2024).
- ¹⁵D. Boiron, A. Michaud, P. Lemonde, Y. Castin, C. Salomon, S. Weyers, K. Szymaniec, L. Cognet, and A. Clairon, *Phys. Rev. A* **53**, R3734 (1996).
- ¹⁶D. Rio Fernandes, F. Sievers, N. Kretzschmar, S. Wu, C. Salomon, and F. Chevy, *Europhys. Lett.* **100**, 63001 (2012).
- ¹⁷A. T. Grier, I. Ferrier-Barbut, B. S. Rem, M. Delehaye, L. Khaykovich, F. Chevy, and C. Salomon, *Phys. Rev. A* **87**, 063411 (2013).
- ¹⁸S. M. Brewer, J.-S. Chen, A. M. Hankin, E. R. Clements, C. W. Chou, D. J. Wineland, D. B. Hume, and D. R. Leibbrandt, *Phys. Rev. Lett.* **123**, 033201 (2019).
- ¹⁹N. Kimura, Priti, Y. Kono, P. Pipatpakorn, K. Soutome, N. Numadate, S. Kuma, T. Azuma, and N. Nakamura, *Commun. Phys.* **6**, 8 (2023).
- ²⁰C. Lyu, C. H. Keitel, and Z. Harman, *Commun. Phys.* **8**, 3 (2025).
- ²¹P. D. Lett, W. D. Phillips, S. L. Rolston, C. E. Tanner, R. N. Watts, and C. I. Westbrook, *J. Opt. Soc. Am. B* **6**, 2084 (1989).
- ²²C. J. Dedman, K. G. H. Baldwin, and M. Colla, *Rev. Sci. Instrum.* **72**, 4055–4058 (2001).
- ²³S. Matyjaśkiewicz, M. H. Szymańska, and K. Góral, *Phys. Rev. Lett.* **101**, 150410 (2008).
- ²⁴A. Kell, M. Link, M. Breyer, A. Hoffmann, M. Köhl, and K. Gao, *Rev. Sci. Instrum.* **92**, 093202 (2021).
- ²⁵Y. Takahashi, T. Shimizu, N. Tanaka, K. Honda, K. Toyoda, and T. Yabuzaki, *Phys. Rev. A* **59**, 3761–3765 (1999).
- ²⁶J. Bechhoefer, *Rev. Mod. Phys.* **77**, 783 (2005).
- ²⁷K. Ogata, *Modern Control Engineering*, 5th ed. (Pearson, Boston, 2010).
- ²⁸P. Horowitz and W. Hill, *The Art of Electronics*, third edition, 20th printing with corrections ed. (Cambridge University Press, Cambridge, New York, 2024).
- ²⁹*Generic Standard on Printed Board Design (IPC-2221)*, Institute for Printed Circuits (IPC), Bannockburn, IL, USA (1998).
- ³⁰Fast Coil Driver Workfiles Repository, <https://github.com/ifquetzal/coildriver> (2025), [Online; accessed 1-March-2025].